JOURNAL OF MATERIALS SCIENCE 32 (1997) 6459–6469

Silicon carbide (Nicalon™) fibre-reinforced borosilicate glass composites: mechanical properties

P. G. KARANDIKAR, T.-W. CHOU*, A. PARVIZI-MAJIDI
Centre for Composite Materials, Department of Mechanical Engineering, University of Delaware, Newark, DE 19716, USA

N. TAKEDA, T. KISHI
Research Centre for Advanced Science and Technology, University of Tokyo, 4-6-1 Komaba, Meguro ku, Tokyo 153, Japan

The objective of this study was to assess the applicability of an extrinsic carbon coating to tailor the interface in a unidirectional Nicalon™–borosilicate glass composite for maximum strength. Three unidirectional Nicalon™ fibre-reinforced borosilicate glass composites were fabricated with different interfaces by using (1) uncoated (2) 25 nm thick carbon-coated and (3) 140 nm thick carbon coated Nicalon fibres. The tensile behaviours of the three systems differed significantly. Damage developments during tensile loading were recorded by a replica technique. Fibre–matrix interfacial frictional stresses were measured. A shear lag model was used to quantitatively relate the interfacial properties, damage and elastic modulus. Tensile specimen design was varied to obtain desirable failure mode. Tensile strengths of Nicalon™ fibres in all three types of composites were measured by the fracture mirror method. Weibull analysis of the fibre strength data was performed. Fibre strength data obtained from the fracture mirror method were compared with strength data obtained by single fibre tensile testing of as-received fibres and fibres extracted from the composites. The fibre strength data were used in various composite strength models to predict strengths. Nicalon–borosilicate glass composites with ultimate tensile strength values as high as 585 MPa were produced using extrinsic carbon coatings on the fibres. Fibre strength measurements indicated fibre strength degradation during processing. Fracture mirror analysis gave higher fibre strengths than extracted single fibre tensile testing for all three types of composites. The fibre bundle model gave reasonable composite ultimate tensile strength predictions using fracture mirror based fibre strength data. Characterization and analysis suggest that the full reinforcing potential of the fibres was not realized and the composite strength can be further increased by optimizing the fibre coating thickness and processing parameters. The use of microcrack density measurements, indentation–frictional stress measurements and shear lag modelling have been demonstrated for assessing whether the full reinforcing and toughening potential of the fibres has been realized.

1. Introduction

In brittle matrix composites the load transfer and, as a result, the mechanical properties depend on the type of bond between the fibre and matrix [1]. If chemical reactions occur at the fibre–matrix interface, a strong interfacial bond results. A strong bond results in good load transfer and high reinforcing efficiency. In this case the interface can be characterized by a "shear strength". However, a strong interfacial bond also results in propagation of cracks from fibre to matrix or *vice versa*. A strong chemical bond at the interface in brittle matrix composites results in brittle behaviour or catastrophic failure, i.e., once the matrix cracks at the critical matrix cracking stress, the cracks easily propagate through the fibres. Therefore, in brittle matrix composites, the interface needs to be weak and be able to debond when a matrix crack approaches.

Of course, too weak an interface will reduce load transfer and reinforcing efficiency. Therefore, the interface characteristics must be optimized. Often, in brittle matrix composites or ceramic matrix composites (CMCs), there is no chemical bond between the fibre and the matrix. The load transfer is achieved only through frictional stress arising from interlocking

* Author to whom all correspondence should be addressed.

0022–2461

of surface aspirities of fibre and matrix. Radial residual stresses produced after cooling from the processing temperature often play a critical role as these decide the normal force on the interface and hence the frictional stress. Such interfaces are characterized by a critical interfacial frictional stress (and not a "shear strength") beyond which fibre and matrix slip relative to each.

Use of such frictional interfaces for producing tough and high strength brittle matrix composites has been demonstrated in Nicalon™ (SiC) fibre-reinforced glass–ceramic matrix composites [2, 3]. In tough, high strength Nicalon™–lithium aluminosilicate (LAS) and Nicalon™–calcium aluminosilicate (CAS) systems a frictional interface is achieved through a predominantly carbon layer formed at the fibre–matrix interface during processing via chemical reactions between the matrix and the Nicalon™ fibres [4–6]. The interface layer in the Nicalon™–LAS system is 40–100 nm thick. The interface layer in the Nicalon™–CAS system is about 10 nm thick and has a small percentage of silica. The interface layer thickness depends on the diffusion controlled chemical reactions and processing conditions. Lack of formation of such a layer at the fibre-matrix interface leads to fibre-matrix chemical reaction, a brittle failure and low tensile strength.

A number of studies on Nicalon™ fibre reinforced borosilicate glass (BSG) composites have been reported in the literature [7–13]. It is observed that the composite strength is very sensitive to processing conditions. In particular, the glass matrix devitrifies to form crystalline cristobalite in the presence of fibres [9] in the temperature range 750 to 950 °C. While BSG has a slightly lower coefficient of thermal expansion (CTE) than Nicalon™ fibre, cristobalite has a much higher CTE. Thus, the formation of cristobalite may lead to residual tensile stresses in the matrix, as well as microcracking and clamping of the fibres, increasing the fibre–matrix interfacial frictional stress. Thus, the fabrication conditions must be chosen to achieve two goals: (1) minimizing devitrification, and (2) formation of an interfacial carbon layer. One feasible approach to this problem is to design an externally deposited coating on the fibres to achieve the desired mechanical behaviour.

For most of the Nicalon™–BSG composites reported in the literature, the failure strain lies between 0.25 and 0.6% and the stress–strain curves are mostly linear. The only notable exception is the data from Habib *et al.* [10] whose composite showed a failure strain of 1.29% and a strength of 725 MPa with a significant non-linear portion in the stress–strain curve.

The objective of this work was to assess the effect of interface design on the tensile strength of Nicalon™–BSG composites.

2. Experimental procedures

The Nicalon™–BSG unidirectional composites were manufactured by Nippon Carbon Co. with dimensions of $100 \times 100 \times 2.0$ mm. The matrix is borosilicate glass (Corning, pyrex #7740). Three types of composites were made: type CG composite has ceramic grade Nicalon™ fibres and type A and B composites have, respectively, 25 and 140 nm carbon coated Nicalon™ fibres [14]. The carbon coating was performed via a chemical vapour deposition process. The composites were made by slurry infiltration and hot pressing. Here, we report characterization results on batches I and II. Batch I was characterized at the University of Delaware and the batch II materials were characterized at the University of Tokyo. Both batches were processed under identical conditions. Details of the interfacial characteristics of these composites can be found in references [14, 15].

The carbon coating thickness chosen correspond to those in Nicalon™–CAS and Nicalon™–LAS systems [4–6]. Here we report the tensile stress–strain behaviour (0°) and damage development in these Nicalon™–BSG composites. Various specimen designs were used to obtain a desirable failure mode in the tensile tests. The fibre–matrix interfacial frictional stress was measured using the indentation technique [16, 17]. A shear lag model [18] was used to infer the extent of interfacial debonding in the composites. The results were compared with similar results previously obtained on Nicalon™–CAS by the authors [18].

The fibre strength distributions in the CG, A and B composites were characterized by the fracture mirror method [19–21]. Observations of the fracture surfaces of the three composites indicated that fibre fractures always initiated from surface flaws. In a brittle fibre, under an applied load, a surface flaw grows, reaches a critical size and then the fibre breaks catastrophically (fast fracture). Crack growth up to the critical size gives rise to a smooth fracture surface (fracture mirror). The region beyond critical size is marked by features such as hackles radiating outwards from the smooth region. Fig. 1 shows the fracture mirror and hackles on the fracture surface of a fibre in composite B-I. The fibre strength, σ, mirror radius, r_m, and fibre fracture toughness, K_f, are related by the following equation [20, 21]:

$$K_f = \sigma(r_m)^{1/2}/A_m \quad (1)$$

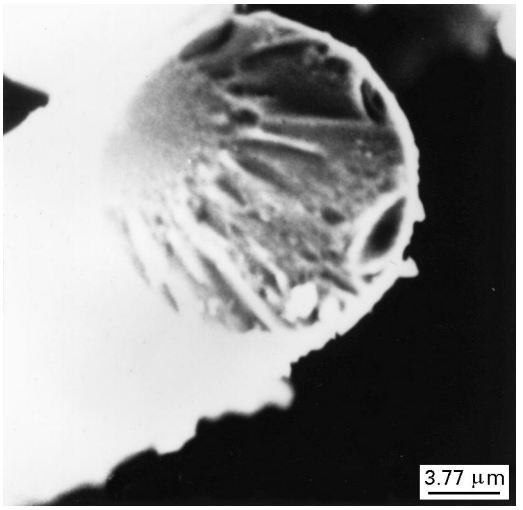

Figure 1 Fracture mirror on the surface of a failed Nicalon fibre in composite B.

where A_m is the mirror constant. Fibres on the fracture surfaces were observed under a scanning electron microscope and high magnification (1500–2000 times) micrographs were obtained. Fracture mirror radii were measured on 30 fibres for each composite. A mirror constant of 3.5 and a K_f value of 1 MPa $m^{1/2}$ [20, 21] was assumed. Fracture mirror sizes (and the toughness) cannot be obtained from single fibre tensile tests since the fibres often shatter into many pieces and the fracture surface cannot be obtained.

These fibre strength distributions obtained by fracture-mirror method were compared to those obtained by single fibre tensile testing at United Technologies Research Centre on fibres extracted from the composites and virgin fibres from spools which were the source for the fibres in the composite. The gauge length for the single fibre tensile testing was 1″ (1″ = 2.54 cm). The strength data were used in various CMC strength models [22–29] to assess their suitability for predicting the strengths of Nicalon™–BSG composites.

Two types of specimens were used for tensile testing: parallel-sided and dog-bone shaped (Fig. 2(a–c)). The nominal dimensions of the parallel-sided specimens were 100 × 10 × 2.0 mm. End-tabs were bonded on to the parallel-sided specimens with an adhesive. The material (glass-epoxy or aluminium) and angle (30 or 15°) of the tabs were varied to achieve different stress concentrations under the tabs. The end-tab length and thickness were 30 and 2 mm, respectively. Tensile testing was carried out in a screw-driven Instron at a crosshead speed of 0.0021 mm s^{-1}. Prior to testing, specimen edges were polished using diamond pastes (1 μm size). Strain gauges (5 mm gauge length) were mounted on to both surfaces of the specimens. Damage on the specimens was recorded using a replica technique. The crack density was measured by a technique described earlier [18]. For comparison purposes Nicalon™–epoxy composites (volume fraction = 0.6) were fabricated and tested and show failure strain and strength values in excess of 1.0% and 1.13 GPa, respectively. Two dog-bone specimens were machined from each batch I composites A and B (Fig. 2c) from 100 × 10 × 2 mm The width of the dog-bone specimens in the gauge section is 1.2 mm and the shoulder radius is 10 mm.

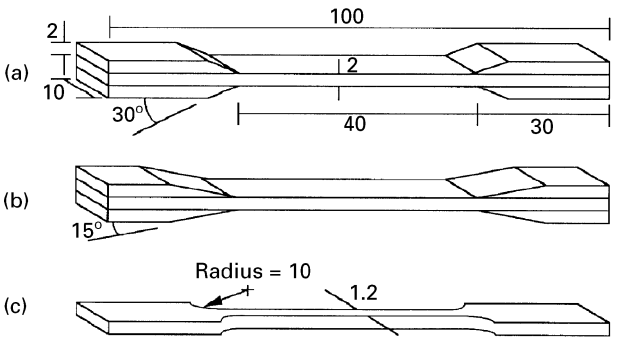

Figure 2 Tensile test specimen geometries (a) parallel-sided specimen with 30° end tabs (b) parallel-sided specimen with 15° end tabs (c) dog-bone specimens.

The fibre–matrix interfacial frictional stresses were determined by the fibre push-in technique using the Vickers microindenter (100 g load) [16, 17]. Ten fibres were pushed in for each type of batch I composite. The dimensions of the indentations on the fibre and matrix and fibre radii were measured on high magnification micrographs obtained by scanning electron microscopy. The fibre hardness is assumed to be 13 GPa (as measured in references [16, 17] on Nicalon fibres).

3. Results and discussion

3.1. Tensile behaviour

The longitudinal stress–strain curves for the Nicalon™–BSG composites of type CG, A and B are compared with that of Nicalon™–CAS [18] in Fig. 3. For comparison, stress–displacement curves for the dog-bone shaped specimens A′ and B′ are also shown. Composite CG shows a very low strength; it fails as soon as first matrix cracking occurs (∼ 0.12% strain). Composites A and B survive first matrix cracking and undergo multiple cracking. The stress–strain curve for composite B shows some non-linearity with a failure strain of ∼ 0.51%. Although the failure of this specimen initiates under the end-tabs, the strength is only slightly lower than that given by the dog-bone specimen. The tensile properties of the composites are summarized in Table 1.

The evolutions of the crack densities in the composites are compared in Fig. 4. Composite CG fails as soon as microcracking begins and hence multiple cracking does not develop. In the Nicalon–CAS composite, crack density reaches a saturation level. On the other hand, failure in composites A and B occurs before microcracking reaches the saturation level. For composites A and B, the crack densities at failure are 4 and 5 cracks per mm, respectively, compared to a saturation density of 7.8 in Nicalon™–CAS [18]. The fibre–matrix interfacial frictional stresses, τ, were calculated from these crack densities using the Aveston, Cooper and Kelly (ACK) model [31, 32] and are listed in Table II.

The fibre–matrix interfacial frictional stresses measured by the indentation technique [16, 17] are also listed in Table II for comparison. The indentation

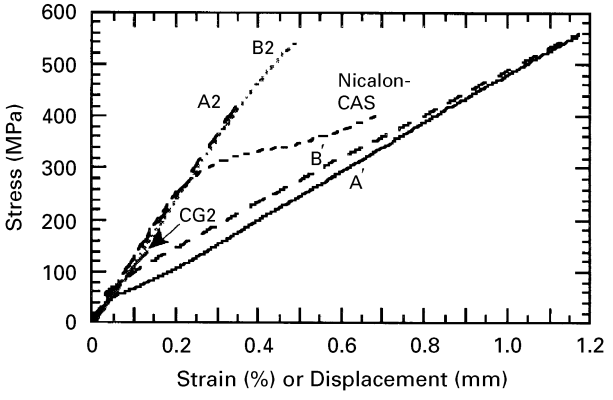

Figure 3 Comparison of the stress-strain curves for unidirectional Nicalon™–BSG composites (A, B and CG) with Nicalon™–CAS [19]. Also shown are the stress-displacement curves for dog-bone specimens A′ and B′.

TABLE I Summary of mechanical properties of Nicalon–BSG composites

Composite	Fibre volume fraction	Young's modulus (GPa)	Poisson's ratio	Matrix cracking stress (0°) (MPa)	Tensile strength (0°) (MPa)	Tensile strength (90°) (MPa)
CG-I	0.39	115.1	0.210	158.8	158.8	—
CG-II	0.38	116.0	—	165.0	165.0	28.0
A-I	0.44	120.7	0.198	207.6	558.1	—
A-II	0.45	124.8	—	202.3	381.8	19.5
B-I	0.45	122.2	0.193	261.6	585.1	—
B-II	0.46	126.1	—	250.0	624.2	28.4

Batch I composites were tested at the University of Delaware and batch II composites were tested at the University of Tokyo

TABLE II Comparison of measured and calculated interfacial frictional stresses (τ)

Composite	Matrix cracking stress (MPa)	Crack spacing (μm)	Calculated τ (MPa)	Experimental τ (MPa)
CG-I	139.7	–	–	287.2 ± 27.6
A-I	207.6	263.2[a]	$\geqslant 5.0$	32.5 ± 4.2
B-I	261.6	191.6[a]	$\geqslant 8.6$	24.7 ± 6.8
A-II	202.3	132.2[a]	$\geqslant 9.7$	–
B-II	250.0	246.5[a]	$\geqslant 6.2$	–
Nicalon–CAS[b]	117.5	129.9	8.4	7.8 ± 1.8

[a] crack spacing may not have reached saturation,
[b] Reference [18]

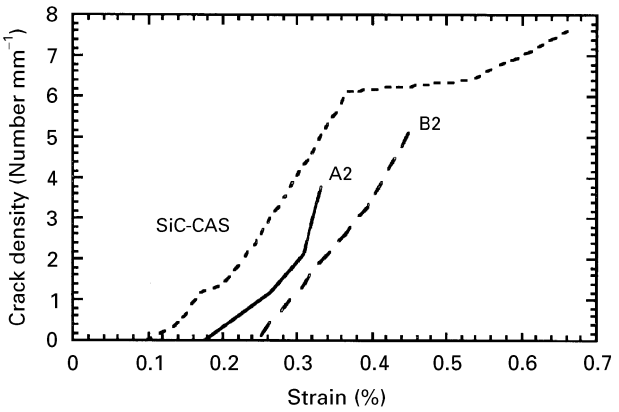

Figure 4 Evolution of crack density in Nicalon™–BSG and Nicalon™–CAS [19] composites.

method used here is applicable for a composite that does not have an interfacial chemical bond (i.e. the stress between the fibre and the matrix occurs only via frictional stresses). Such a condition can be assumed in composites A and B due to the extrinsically deposited carbon coating on the fibres and in the Nicalon–CAS composite due to the carbon interface produced during processing. In the indentation method the model used for extracting frictional stress from dimensions of indentations requires that the length over which the fibre slips be much greater than the fibre radius. Here, the calculated ratio of fibre slip distance [17] to the fibre radius is found to be of the order of 45, which satisfies the above requirement. Also, since the indentation test loads the fibres in compression, the fibres expand in the transverse direction due to Poisson's effect, causing overestimation of τ.

Nevertheless, the experimental and calculated frictional stresses compare very favourably for the Nicalon–CAS composite. The calculated frictional stresses for composites A and B, on the other hand, are lower than the experimental ones because failure in A and B composites occurred before microcracking reached saturation (whereby the crack spacing would decrease further). The measured interfacial frictional stress of the CG composite (287 MPa) is very high compared to that of composites A (32.5 MPa) and B (24.7 MPa), indicating a very strong bond between the fibre and the matrix in composite CG (and inapplicability of the simple frictional model). This result is consistent with the experimental observed fact that the composite failed as soon as first matrix cracking occurred. The fibre coating approach seems to be successful in imparting a frictional characteristic to the interface as desired. The interfacial frictional stress for composite B (140 nm carbon coating) is lower than that of composite A (25 nm carbon coating). Thus, the interfacial frictional stress reduced as the coating thickness increased. At this point it is interesting to compare the frictional stresses measured in composites A and B with those measured on other systems that show high strength and toughness. For example, the interfacial frictional stress in Nicalon™–CAS composite was 8–12 MPa, whilst in the Nicalon™–LAS composite it was 2 MPa and in the Nicalon™–BSG composite it was 2–8 MPa [10, 12]. In particular, the Nicalon™–BSG composite in reference [10] which showed high tensiles strength (and failure

strain), has a frictional stress of 2 MPa. Thus, the interfacial frictional stress in composites A and B investigated in this study is higher than that of high-strength composites reported in the literature.

A shear lag model [18] was used to predict the modulus degradation in the B composite. In this model the fibre and matrix are modelled as concentric cylinders. The composite modulus is calculated as a function of matrix crack spacing (l) and debond length (S_d). A frictional stress transfer from fibre to matrix is assumed in the debonded region. Experimentally measured crack densities are used as input for the model and the debond length is increased gradually. When S_d reaches $l/2$, the entire interface is debonded. The experimental modulus variation is compared with theoretical predictions in Fig. 5. The comparison indicates that around 30% of the fibre–matrix interface has debonded at failure. Similar comparisons for Nicalon™–CAS [18] indicated a completely debonded interface at saturation microcracking. The limited extent of debonding in the B composite is consistent with the measured high fibre–matrix interfacial frictional stress. The interface in composite B can be further optimized (by lowering the frictional stress further) to allow cracking to develop to saturation level, debonding to develop further and in turn give a composite with even higher failure strain and strength.

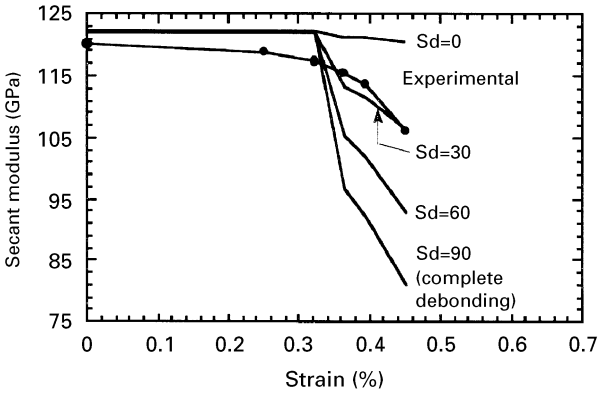

Figure 5 Prediction of modulus reduction in *B* composite by shear lag model (S_d-debond length in crack spacing at failure 180 μm).

The effect of specimen design on the failure mode and failure strain are summarized in Table III. Three specimens of each type were tested. The failure modes observed in these specimens are shown in Fig. 6. The data in Table III show that for the Nicalon™–CAS composites glass-epoxy end-tabs with 30° taper give a failure strain (0.75%) that is very close to that obtained using a dog-bone specimen (0.8%) [33]. In the end-tabbed specimen failure does initiate under the tabs by interlaminar shear but a significant portion of the failure is tensile.

For the 30° glass-epoxy end-tabbed specimen of composite CG, failure initiated under the tabs (Fig. 6: Type CG(a)). Gauge section failure was obtained using 15° glass-epoxy end-tabs (Fig. 6: Type CG(b)). In both the CG cases the failure was completely brittle with no fibre pull out (Figs. 7a and 8a). The brittle failure mode and the low strength is consistent with the high measured frictional stress, indicating a strong interface. Glass-epoxy end-tabs with a 30° angle resulted in significantly different failure modes (and low failure strain) in composites A and B compared to Nicalon™–CAS. In A and B, specimen failure occurred by splitting and/or delamination which initiated under the tabs (Fig. 6: Type A(a), Type B(a)).

In composite B, as the end-tab design was changed to 15° tapered glass-epoxy, the extent of splitting reduced (Fig. 6: Type B(b)) and the failure strain (and strength) increased. With 15° aluminium end-tabs the splitting was completely eliminated, the failure strain increased and the failure mode resembled that of Nicalon™–CAS with 30° glass-epoxy end-tabs (Fig. 6: Type B(c)). Similar changes in the end-tabs for the type A composite did not reduce the extent of splitting and the failure mode was as depicted by Fig. 6: Type A. Correspondingly, in composite A the failure strain did not increase. These observations suggest that the splitting failure mode is undesirable and should be eliminated to increase the measured tensile strength.

TABLE III Effect of specimen design on failure strain (ε*), strength (σ*) and failure mode

Composite	Property	Glass-epoxy end-tabs		Aluminium end-tabs 15°	Dog-bone	
		30°	15°			
CG-I	ε*	0.1278	0.1431	–	–	
	σ* (MPa)	139.7	158.8	–	–	
	Failure	1	2	–	–	
A-I	ε*	0.3743	0.3404	0.3209	–	–
	σ* (MPa)	434.9	401.9	387.2	347.5	558.1
	Failure	3	3	3	7	6
B-I	ε*	0.3588	0.4427	0.5181	–	–
	σ* (MPa)	440.6	490.2	547.0	585.1	556.5
	Failure	3	4	5	6	6
Nicalon–CAS[a]	ε*	0.7547	–	–	0.8000	
	σ* (MPa)	398.0	–	–	325.0	
	Failure	5	–	–	6	

1. Brittle (no pull out) under tabs, 2. Brittle in gauge section, 3. Splitting Fig. 6, Type A – (a), (b) and (c) 4. Limited splitting, delamination and tensile Fig. 6, Type B – (b) 5. Delamination and tensile Fig. 6, Type B – (c) 6. In gauge section with pull out, and 7. Failure in the neck region.
[a] References [18, 33].

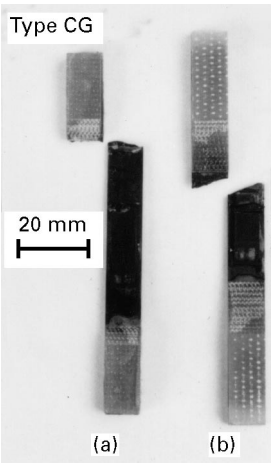

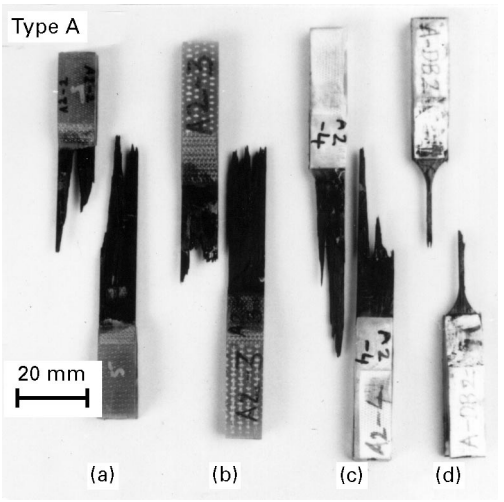

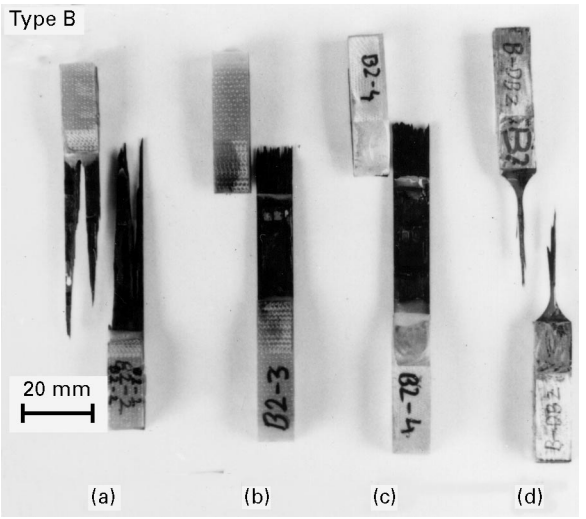

Figure 6 *Specimen designs*: all (a) have 30° glass-epoxy end tabs, all (b) have 15° glass-epoxy end tabs, all (c) have 15° aluminium end tabs and all (d) are dog-bone with 15° aluminium end tabs; *Failure modes*: Type CG (a) brittle inside tabs, (b) brittle in the gauge section Type A (a), (b) and (c) splitting and/or delamination, (d) gauge section; tensile failure with pull out; Type B (a) splitting, (b) and (c) limited splitting, delamination and tensile and (d) gauge section tensile failure with pull out.

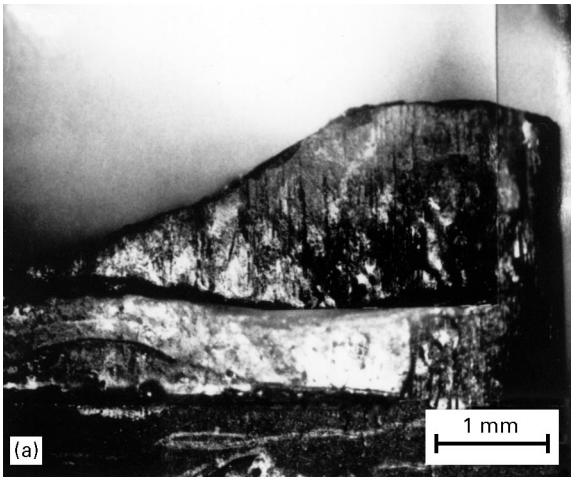

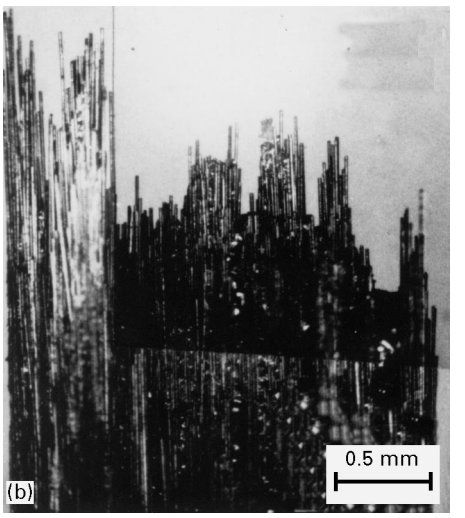

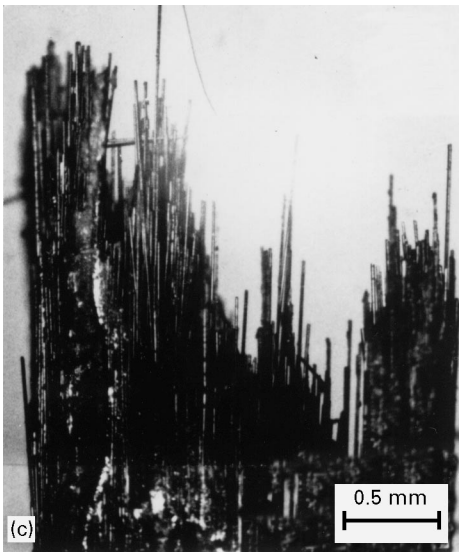

Figure 7 Failed Nicalon-BSG composites: (a) CG – brittle failure, (b) A – fibre pull out, (c) B – fibre pull out.

The reinforcement in the glass-epoxy end-tabs is in the form of a plane woven fabric. The Poisson's ratio for this material is very low as the traverse fibres prevent lateral contraction. The Poisson's ratio for unidirectional composite, on the other hand, is high. This mismatch produces through-the-thickness tensile stresses in the composite under the end-tabs. The Poisson's ratio of aluminium, on the other hand, is closer to that of a unidirectional Nicalon™–BSG composite. Therefore, lower mismatch stresses are

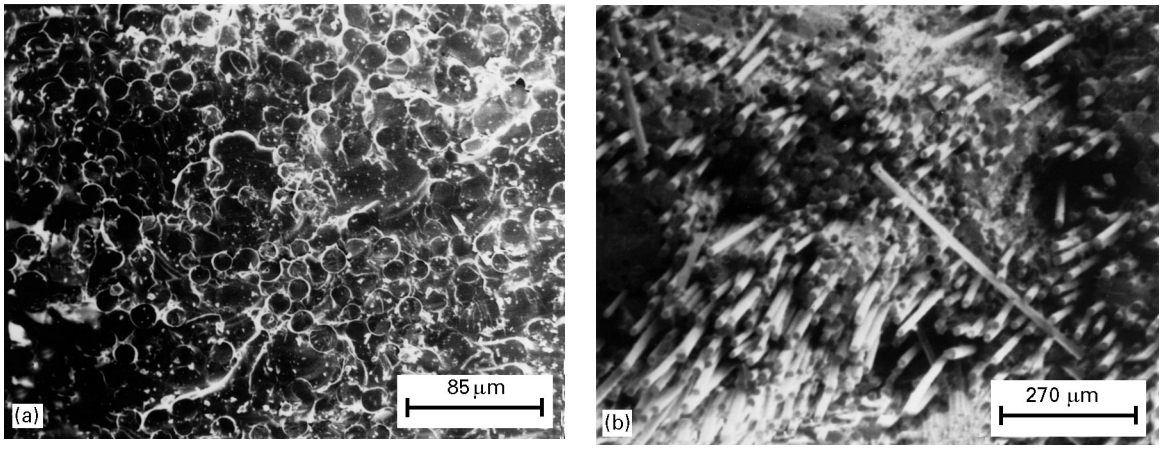

Figure 8 Scanning electron micrographs showing (a) flat fracture in composite CG and (b) fibre pull out in composite B.

produced under the tabs. In an end-tabbed specimen load is transferred from the tabs to the specimen via shear stresses (interlaminar). In parallel-sided end-tabbed specimens, interlaminar normal and shear stresses (and stress concentrations at the end of the tab) have been shown to occur [34, 35] through finite element analysis. It has been shown that as the angle of the tab is reduced, the stresses are reduced substantially.

These calculation are confirmed by our experimental data on composite B for which reducing the angle of the tabs and changing the tab material prevented splitting failure and postponed the interlaminar shear failure by lowering the stresses under the tabs. A similar change in the specimen design, however, did not improve the strength of composite A. This may happen if composite A has lower through-the-thickness tensile strength, through-the thickness shear strength or in-plane shear strength than the respective strengths in composite B and the stresses under the tabs in composite A are still higher than the respective composite A strengths. The through-the-thickness (or 90°) tensile strength of composite A was (20 MPa) indeed lower than that of composite B (28 MPa).

Two dog-bone tensile specimens each were tested for both the A-I and B-I samples. For material A, one of the specimens failed in the shoulder region by splitting and hence showed a lower strength. The other specimen showed gauge section tensile failure with pull out (Figs. 6: Type A(d), and Fig. 7b). The strength of this specimen is 558.1 MPa. Both of the dog-bone specimens of composite B-I showed gauge section tensile failure (Fig. 6: Type B(d) and also Figs. 7c and 8b) with strengths of 585.1 and 556.5 MPa. Thus, the parallel sided 15° aluminium end-tabbed specimen of composite B shows a strength (547.0 MPa) that is very close to that obtained with the dog-bone specimens. Although composites A and B both show pull out, in composite A fibres pull out in groups and the pull out lengths (average 0.13 mm) are smaller than those in B (average 0.84 mm).

3.2. Fibre strength measurements

Fracture mirror data were obtained (for batch I composites) from the fracture surfaces of the dog-bone specimens of A and B and parallel-sided end-tabbed (15°, glass-epoxy) specimens of CG. Fibre strengths calculated by the fracture-mirror method are shown in Fig. 9(a–f). Weibull analysis of the data sets was performed and the corresponding linearized Weibull plots are also shown in Fig. 9(a–f). Superposed on the fracture mirror strength data are the strength data obtained by single fibre tensile testing of virgin and extracted fibres. The average fibre strengths and Weibull shape and scale parameters for the three composites are summarized in Table IV. Shapes of all the three strength distributions for fibres in each type of composite are similar, as is evident in very similar Weibull shape parameters. The scale parameter, on the other hand, change-significantly between the as-received, extracted and fracture mirror data. It is interesting to note here that the shape parameter values (4.4–6.1) and scale parameter values (2045–2466 MPa) obtained in this study by the fracture mirror method on fibres in the Nicalon™–BSG composite are very similar to those obtained for fibres in the Nicalon™–LAS composite reported by Bleay and Scott [12] who also, used the fracture mirror method.

Both the extracted single fibre strengths and the strengths calculated on the basis of the fracture mirror method are lower than the virgin fibre strengths; thus the fibre strength is obviously degraded after incorporation into the matrix and processing. In particular, the ratios of extracted fibre strength to as received fibre strength are 0.49, 0.45, and 0.38 in the CG, A and B composites, respectively. The extracted single fibre strengths are consistently lower than the mirror analysis-based strength data in all three composites. The possible reasons for this phenomenon are: (i) the assumed mirror constant, (ii) the assumed fracture toughness and (iii) fibre degradation that may occur during the extraction process.

3.3. Prediction of the composite ultimate tensile strength

Some generic composite strength models [22–24, 30] and some models specifically developed for CMCs [20, 25–29] have been adapted to the prediction of the strength of the Nicalon™–borosilicate glass

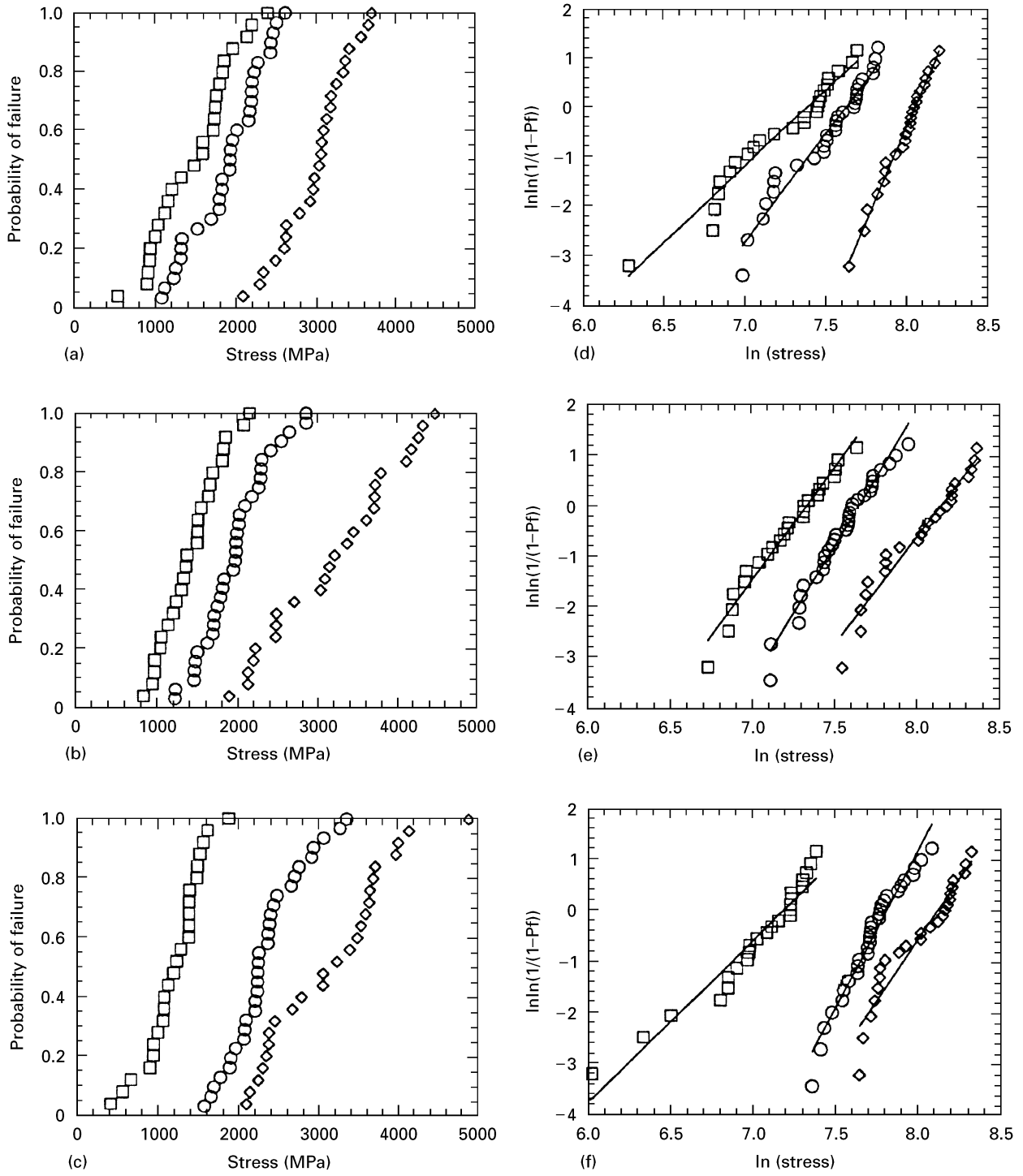

Figure 9 Fibre strength distributions; (□) extracted, (○) fracture mirror analysis and (◇) as-received for (a) CG, (b) A and (c) B composites and also the corresponding linearized Weibull plots for (d) CG, (e) A and (f) B composites, (P_f-probability of failure).

TABLE IV Fibre strength data obtained by fracture mirror analysis and single fibre testing

Composite	Fracture mirror			Extracted single fibre[a]			As-received single fibre[a]		
	m	σ_f	σ^*	m	σ_f	σ^*	m	σ_f	σ^*
CG-I	4.4	1887.8	2044.8	3.1	1472.5	1612.3	7.6	2986.5	3138.9
A-I	5.4	1967.7	2098.8	4.4	1425.3	1527.5	4.3	3196.4	3453.4
B-I	6.1	2327.6	2465.7	3.2	1196.2	1315.8	4.7	3145.1	3365.5
Nicalon–CAS	–	–	–	4.7	1448.0	1535.3	–	–	–

m, σ^* – Weibull shape and scale parameters, σ_f – average fibre strength, [a] tests conducted at United Technologies Research Centre (gauge length 25.4 mm), strength in MPa

composites. The fibre strength data obtained by the fracture mirror method and extracted single fibre tensile testing data are used in various models to predict the ultimate tensile strength (UTS) of the three composites and the predictions are then compared with the experimental data in Tables V and VI, respectively. A brief discussion of the strength models used follows.

The average fibre strength model assumes that the matrix contribution to the strength is negligible, the fibre strength is single valued, and also that fibre failures are non-interactive. For average fibre strength, σ_f, the composite strength, S_A, is given by:

$$S_A = \sigma_f V_f \tag{2}$$

The fibre bundle model [22] takes the fibre statistical strength distribution into account. Low strength fibres break first, transferring their load uniformly to unbroken fibres. The stress on the unbroken fibres is then higher than the average bundle stress. The bundle as a whole fails when the unbroken fibres are unable to sustain the load. In this model the fibre stress is assumed to be uniform and the fibre failure is assumed to be non-interactive. The fibre bundle strength, σ_B, and the composite strength, S_B, are given by:

$$\frac{\sigma_B}{\sigma_f} = \left(\frac{1}{me}\right)^{\frac{1}{m}} \frac{1}{\Gamma\left(1+\frac{1}{m}\right)} \qquad S_B = \sigma_B V_f \tag{3}$$

where Γ denotes the gamma function, m is the Weibull shape parameter and e is the base of natural logarithm. The bundle strength is lower than the average fibre strength and it reduces as the variation in fibre strength increases (lower m).

The cumulative fibre failure model [23, 24] is very similar to the bundle model except that stress near a fibre break is assumed to be non-uniform and is taken into account through an ineffective length, L_C, within the gauge length, L. The cumulative fibre bundle strength, σ_C, and the composite strength, S_C, are given by:

$$\frac{\sigma_C}{\sigma_B} = \left[\frac{L}{L_C}\right]^{\frac{1}{m}} \qquad S_C = \sigma_C V_f \tag{4}$$

Contrary to bundle strength, cumulative strength exceeds the average fibre strength. The ineffective length is difficult to estimate and it is assumed to be equal to the average pull out length measured on the fracture surfaces (0.84 and 0.13 mm for composites B and A, respectively). No pull out is observed in CG specimens and hence cumulative fibre failure model-based predictions are not carried out for CG specimens.

Recently, some models have been proposed specifically for CMCs by considering the damage development. One such model is that developed by Cao and Thouless [25]. It is based on an earlier model proposed by Thouless *et al.* [20]. In the Cao–Thouless model, the composite after saturation microcracking is considered. Fibre strength variability is taken into account and fibre stress distribution is calculated by a shear lag analysis. Fibre failure is assumed non-interactive, and multiple fibre failure is neglected. The composite strength, S_{CT}, is given by:

$$S_{CT} = V_f \Sigma \left[\frac{\Sigma R}{m(m+1)\tau L}\right]^{\frac{1}{m}} \exp(-1/m) \tag{5}$$

where

$$\Sigma = \left[\frac{A_0 S_0^m \tau (m+1)}{2\pi R^2}\right]^{\frac{1}{m+1}}$$

$$S_0 = \sigma^* \left[\frac{2\pi RL}{A_0}\right]^{\frac{1}{m}}$$

σ^* is the Weibull scale parameter, L is the gauge length, R is the fibre radius and A_0 is a normalizing factor ($= 1\,m^2$). Algebraic manipulations show that the strength predicted by this model is independent of τ.

TABLE V UTS predictions using fracture mirror-based fibre strength data

Composite	Exp.	S_A	S_B	S_C	S_{CT}	S_{CRT}		
						Exp. τ	$\tau = 10$	$\tau = 1$
CG-I	158.8	736.2	458.7	–	453.7	1703.5	914.8	597.2
A-I	558.1	865.8	569.9	1510.2	561.5	1212.0	1008.9	703.5
B-I	585.1	1047.4	710.8	1243.9	700.2	1248.6	1099.3	794.8

Strength in MPa

TABLE VI UTS predictions using extracted single fibre strength data

Composite	Exp.	S_A	S_B	S_C	S_{CT}	S_{CRT}		
						Exp. τ	$\tau = 10$	$\tau = 1$
CG-I	158.8	574.3	322.8	–	316.0	1960.8	864.7	492.2
A-I	558.1	627.1	392.6	1295.6	383.7	1015.3	816.2	532.9
B-I	585.1	538.3	305.3	885.4	300.6	1042.7	840.7	485.9
Nicalon–CAS	445.8	506.8	321.2	–	311.8	669.0	698.8	466.6

Strength in MPa

Curtin [26] has proposed a model with assumptions similar to those in the Cao–Thouless model but allowing for multiple fibre failures. The composite strength, S_{CRT}, is given by:

$$S_{CRT} = V_f \sigma \left[\frac{2}{m+2}\right]^{\frac{1}{m+1}} \frac{m+1}{m+2} \quad (6)$$

where

$$\sigma = \left[\frac{A_0 \sigma_0^m \tau L_0}{R}\right]^{\frac{1}{m+1}}$$

L_0 is the fibre length, and σ_0 is the stress at which 63.2% of the fibres fail. According to this model the composite strength is proportional to $\tau^{1/(m+1)}$. Thus, the strength can vary substantially with τ, especially for low m values. Therefore, predictions with this model are made at measured τ as well as $\tau = 1$ and 10 MPa to demonstrate this effect.

Since the CG composite fails in a brittle fashion without multiple cracking the models are really not applicable and the strengths are highly over-predicted. If fibre strength distributions obtained by fracture mirror analysis are used, predictions of the bundle model and the Cao–Thouless model are closest to the experimental value. On the other hand, if the extracted fibre strength data are used, the average strength model gives the best predictions. In this case, the composite strength is underestimated by the bundle theory and the Cao–Thouless model. For both fibre strength data sets the composite strengths are overestimated by the Curtin model if the measured interfacial frictional stresses are used. The predictions by this model are much closer to the experimental values if a frictional stress of the order of 1 MPa is used. It can be seen that in all the cases, the predictions of the Cao–Thouless model differ only slightly from those of the bundle model. It also should be noted that these composites may not have developed saturation microcracking before failure. Therefore, the strength predictions by the last two models could be inaccurate.

4. Conclusions

In the absence of an interfacial coating, Nicalon™–BSG composite specimens broke catastrophically as soon as the first matrix cracking occurred, and thus no toughening was achieved. Extrinsically deposited interfacial carbon coating successfully imparted a frictional characteristic to the fibre–matrix interface. For the carbon coating thicknesses investigated, the interfacial frictional stress reduced as the coating thickness increased. The coated fibre composites survived first matrix cracking and showed multiple cracking. Nicalon™–BSG composite specimens with a strength as high as 585 MPa were fabricated using a 140 nm thick extrinsically deposited carbon coating on the fibres. However, matrix microcracking in this composite did not reach a saturation level at failure and interfacial frictional stress in this composite is higher than that in some higher-strength composites reported in literature. Thus, the coating thickness and processing must be further optimized to improve the tensile strength of the composite. The composite through-the-thickness tensile and in-plane and through-the-thickness shear strengths played a very significant role in determining the failure mode and the measured tensile strength of the composite when end-tabbed specimens were used.

The extracted single fibre strengths were consistently lower than the mirror analysis-based strength data in all three composites. This difference may be attributed to the assumed mirror constant, assumed fracture toughness and damage during extraction. Both fracture mirror analysis and extracted single fibre tensile test data reveal that significant fibre strength degradation occurs during processing. Since the fracture mirror analysis and the single fibre tests give different fibre strength distributions, different model predictions are obtained based on each data set and one particular model cannot be singled out as "applicable." In all these cases, the predictions of the Cao–Thouless model differ only slightly from those of the bundle model.

Thus, this study has demonstrated the successful use of extrinsic carbon coatings for fabricating tough, high-strength Nicalon™–BSG composite. Also, the use of micro-crack density measurements, indentation-frictional stress measurements and shear lag modelling has been demonstrated for assessing whether or not the full reinforcing and toughening potential of the fibres has been realized.

Acknowledgements

The funding for this work is provided by the New Energy and Industrial Technology Development Organization (NEDO) of Japan through an International Joint Research Programme. The composites were supplied by Nippon Carbon Co. The input from the other partner in this project, United Technologies Research Centre (Dr. Karl Prewo and Dr. Bill Tredway), is also appreciated.

References

1. P. G. KARANDIKAR and T.-W. CHOU, in "Handbook on Continuous fibre-reinforced ceramic matrix composites", edited by R. L. Lehman, S. K. El-Rahaiby and J. B. Wachtman, Jr. (CIAC and *American Ceramic Society*, Westerville, Ohio, 1995) pp. 355–429.
2. J. J. BRENNAN and K. M. PREWO, *J. Mater. Sci.* **17** (1982) 2371.
3. K. M. PREWO, J. J. BRENNAN and G. K. LAYDEN, *Ceram. Bull.* **65** (1986) 305.
4. J. J. BRENNAN, in "Tailoring multiphase and composite ceramics", edited by Tresseler et al. (Plenum Press, New York, 1986) pp. 549–560.
5. R. F. COOPER and K. CHYUNG, *J. Mater. Sci.* **22** (1987) 3148.
6. L. A. BONNEY and R. F. COOPER, *J. Amer. Ceram. Soc.* **73** (1990) 2916.
7. K. M. PREWO and J. J. BRENNAN, *J. Mater. Sci.* **15** (1980) 463.
8. A. BRIGGS and R. W. DAVIDGE, *Mater. Sci. Engng.* **A109** (1989) 363.
9. V. S. R. MURTY and M. H. LEWIS, *J. Mater. Sci. Lett.* **8** (1989) 571.
10. F. A. HABIB, R. G. COOKE and B. HARRIS, *Brit. Ceram. Trans. J.* **89** (1990) 115.

11. H. HEGELER and R. BRUCKNER, *J. Mater. Sci.* **25** (1990) 4836.
12. S. M. BLEAY and V. D. SCOTT, *ibid.* **26** (1991) 2229.
13. V. RAMAKRISHNAN and N. JAYARAMAN, *ibid.* **27** (1992) 2423.
14. W. TREDWAY, K. M. PREWO, in Proceedings 3rd Japan Int. SAMPE Symposium, Tokyo, 1993, edited by T. Kishi, N. Takeda and Y. Kagawa (Japan SAME, Tokyo, December 1993) pp. 531–536.
15. M. UMEZAWA, Y. IMAI and H. ICHIKAWA, *ibid.* pp. 526–530.
16. D. B. MARSHALL, *J. Amer. Ceram. Soc.* **67** (1984) C259.
17. D. B. MARSHALL, B. N. COX and A. G. EVANS, *Acta Metall* **33** (1985) 2013.
18. P. G. KARANDIKAR and T-W. CHOU, *Compos. Sci. Technol.* **46** (1992) 253.
19. J. J. MECHOLSKY, S. W. FREIMAM and R. W. RICE, *J. Mater. Sci.* **11** (1976) 1310.
20. M. D. THOULESS, O. SBAIZERO, L. S. SIGL and A. G. EVANS, *J. Amer. Ceram. Soc.* **72** (1989) 525.
21. D. SINGH and J. P. SINGH, *Ceram. Engng. Sci. Proc.* **13** (1992) 257.
22. B. D. COLEMAN, *J. Mech. Phys. Solids* **7** (1958) 60.
23. B. ROSEN, "*Mechanics of composite strengthening*" (ASM, Metals Park, OH, 1965). Ch. 3.
24. K. M. PREWO, *J. Mater. Sci.* **21** (1986) 3590.
25. H. CAO and M. D. THOULESS, *J. Amer. Ceram. Soc.* **73** (1990) 2091.
26. W. CURTIN, *ibid.* **74** (1991) 2837.
27. M. SUTCU, *Acta Metall.* **37** (1989) 651.
28. H. R. SCHWEITERT and P. S. STEIF, *J. Mech. Phys. Solids* **38** (1990) 325.
29. K. M. KNOWLES and X. F. YANG, *Ceram. Engng. Sci. Proc.* **12** (1991) 1375.
30. T.-W. CHOU, "*Microstructural design of fibre composites*", (Cambridge University Press, Cambridge, UK, 1992).
31. J. AVESTON, G. A. COOPER and A. KELLY, in "The properties of fibre composites", (IPC Science and Technology Press Ltd., London, 1971) pp. 15–26.
32. A. C. KIMBLER and J. G. KEER, *J. Mater. Sci. Lett.* **1** (1982) 353.
33. S-W. WANG and A. PARVIZI-MAJIDI, *J. Mater. Sci.* **27** (1992) 5483.
34. B. C. FOOS, W. E. WOLFE and R. S. SANDHU, in "Composite materials testing and design", Vol. 10., edited by G. C. Grimes, ASTM STP 1120 (American Society for Testing and Materials, Philadelphia PA, 1992) pp. 103–113.
35. M. E. CUNNINGHAM, S. V. SCHOULTZ and J. M. TOTH Jr., in "Recent advances in composites in the United States and Japan", edited by J. R. Vinson and M. Taya, ASTM STP 864 (American Society for Testing and Materials, Philadelphia PA, 1985) pp. 253–262.

Received 30 September 1996
and accepted 4 April 1997